

1 **Revision 1 (Correction date: June 10, 2014)**

2

3 **Optical absorption spectroscopy study of the causes for color variations in natural Fe-bearing**
4 **gahnite: insights from iron valency and site distribution data**

5 Rosa Anna Fregola^{1,*}, Henrik Skogby², Ferdinando Bosi^{2,3}, Veronica D'Ippolito³, Giovanni B.

6 Andreozzi³ and Ulf Hålenius²

7 ¹Dipartimento di Scienze della Terra e Geoambientali, Università di Bari Aldo Moro, via E. Orabona 4,
8 I-70125 Bari, Italy

9 ²Department of Geosciences, Swedish Museum of Natural History, SE-10405 Stockholm, Sweden

10 ³Dipartimento di Scienze della Terra, Sapienza Università di Roma, Piazzale Aldo Moro 5, I-00185
11 Roma, Italy

12

13 **Abstract**

14 Four gahnite single crystals with variable colors from pale blue to green have been studied by a multi-
15 analytical approach with the aim to evaluate existing assignments of optical absorption bands.
16 Combined information from electron microprobe analyses, Mössbauer spectroscopy, IR-spectroscopy,
17 single crystal X-ray structure refinements and optical absorption spectroscopy confirms the conclusions
18 of earlier studies that the absorption bands recorded in the visible spectral region up to ~540 nm (above
19 ~18500 cm⁻¹) are related to electronic *d-d* transitions in tetrahedrally coordinated Fe²⁺. It also
20 demonstrates that a set of absorption bands between ~550-625 nm (~16000-18200 cm⁻¹) are caused by
21 spin-allowed and spin-forbidden *d-d* transitions in tetrahedrally coordinated Co²⁺. Two absorption
22 bands at higher wavelengths (~680 and ~800 nm, i.e. ~14700 and ~12500 cm⁻¹) are assigned to
23 electronic transitions in exchange coupled ^{VI}Fe³⁺-^{IV}Fe²⁺ pairs and a band at ~950 nm (~10500 cm⁻¹) is

* E-mail: rosaanna.fregola@uniba.it

24 assigned to a spin-allowed electronic transition in $^{VI}Fe^{2+}$. Low-Fe gahnite crystals owe their blue color
25 to traces of cobalt at concentration levels in the order of 200 ppm and less, while the green color of
26 gahnite crystals with higher Fe-contents is due to a combination of electronic ligand-metal transitions
27 causing strong UV-absorption and electronic transitions in exchange coupled Fe^{2+} - Fe^{3+} cation pairs that
28 absorb in the red region of the visible spectrum. A detailed characterization of samples that includes
29 cation site occupancy and iron valency data is demonstrated to be crucial for interpreting optical
30 absorption spectra. Also electronic transitions in trace element chromophores below the detection limit
31 of electron microprobe may participate to light absorption. All this information contribute to the
32 comprehension of the causes of crystal color of minerals, gemstones and ceramic pigments.

33

34 **Keywords:** Crystal structure, site occupancy, optical absorption spectra, Mössbauer spectra, spinel,
35 gahnite

36

37

Introduction

38 Spinel oxides are a wide group of minerals and compounds whose peculiar crystal chemistry,
39 compositional flexibility and physical properties make them suitable for a wide range of applications,
40 in Earth Sciences (e.g. as petrogenetic indicators) as well as in Materials Science (e.g. as refractory
41 materials). In particular, the Zn-content of zincian spinels - i.e., gahnite (ZnAl_2O_4), Zn-bearing
42 hercynite (namely, FeAl_2O_4) and Zn-bearing spinel sensu stricto (namely, MgAl_2O_4) - can be used as
43 an exploration guide for metamorphosed base-metal sulphide ores, and Zn-rich spinels are indicators of
44 low-metamorphic grade and high oxygen and sulfur fugacity conditions (e.g. Spry and Scott 1986;
45 Heimann et al. 2005). Synthetic ZnAl_2O_4 spinel finds application, for example, as catalyst and catalyst-
46 support (e.g. Valenzuela et al. 1997) due to its high thermal stability, low acidity, mechanical resistance
47 and hydrophobic behavior. It can be used also in glaze layers of white ceramic tiles to improve wear
48 resistance, mechanical properties and whiteness (e.g. Escardino et al. 2000).

49 The minerals of the very large spinel oxide group usually crystallize in space group $Fd\bar{3}m$. The
50 spinel structure is based on a nearly cubic close-packed arrangement of oxygen atoms, with
51 tetrahedrally (T) and octahedrally (M) coordinated sites and it can accommodate a large number of
52 cations of different valence states. The MO_6 octahedra share half of the edges with neighbouring MO_6
53 octahedra, and corners with TO_4 tetrahedra, but the latter are isolated from each other. The T and M
54 sites are filled by A and B cations, where A and B are mainly divalent and trivalent cations,
55 respectively. The general formula for the cation distribution in the spinel structure is $^{\text{IV}}[\text{A}_{(1-i)}\text{B}_i]^{\text{VI}}[\text{A}_i\text{B}_{(2-i)}]\text{O}_4$,
56 where i is the inversion parameter and IV and VI are the coordination number of T and M sites,
57 respectively. Two ordered configurations are stable at low temperature: normal spinels with $i = 0$ and
58 inverse spinels with $i = 1$. With increasing temperature, the cation distribution of both normal and

59 inverse spinels tends to disorder towards the random configuration of maximum entropy with $i = 2/3$
60 (O'Neill et al. 2005).

61 End-members gahnite, hercynite and spinel sensu stricto (s.s.) are normal spinels. However,
62 unlike Fe-Al and Mg-Al, the intersite exchange Zn-Al is not energetically favored and the synthetic
63 end-member gahnite shows a very limited increase in i from 0.01 at 900°C to 0.05 at 1300°C (O'Neill
64 and Dollase 1994). Natural crystals of end-member gahnite are very rare, as minor replacements of Zn
65 by Fe^{2+} , Mg^{2+} , Mn^{2+} , Fe^{3+} , and Co^{2+} are common (Spry and Scott 1986). Natural Zn-rich samples
66 approaching the ideal gahnite composition are reported in literature, the highest ones having gahnite
67 components of 94-99 mol% (Yalçın et al. 1993; Henry and Dutrow 2001; D'Ippolito et al. 2013).

68 Natural colorless to light blue-green gahnites, with very low Fe- and Mg-contents, are unusual
69 and differ in color to most gahnites, which are reported as dark green to brown (Appel 2000). In the
70 early study by Anderson and Payne (1937) the blue color of natural gahnite crystals was ascribed to the
71 presence of Fe^{2+} cations. In a gemological study of blue Nigerian gahnite crystals, Jackson (1982)
72 noted that they changed their color to a permanent blue-green on heating to 1000°C, whereas they
73 became olive-green at 1400°C. The author speculated that the color change from blue to green could be
74 due to iron oxidation. The causes of color in natural iron bearing spinel s.s. and gahnite single crystals
75 were investigated also by Schmetzer et al. (1989), Taran et al. (2005) and D'Ippolito et al. (2013).
76 Optical absorption spectra of synthetic and natural crystals on the spinel-hercynite join have been
77 presented in several studies (e.g., Gaffney 1973; Slack 1964; Dickson and Smith 1976; Hålenius et al.
78 2002).

79 The optical absorption spectra of natural as well as synthetic Fe-bearing spinels with high
80 $\text{Fe}^{2+}/\text{Fe}^{3+}$ -ratios recorded in previous studies show a set of relatively weak and sharp absorption bands
81 between ca. 18000 cm^{-1} and the UV-edge (between ~ 25000 and ~ 30000 cm^{-1} depending on sample Fe-
82 concentration and thickness). Most authors agree on the assignment of the majority of these absorption

83 bands to spin-forbidden electronic $d-d$ transitions in tetrahedrally coordinated Fe^{2+} ($^{\text{IV}}\text{Fe}^{2+}$). In spectra
84 of Fe^{2+} -dominant and Fe^{3+} -bearing spinels, three relatively weak absorption bands in this spectral
85 region (at ~ 22900 , ~ 21500 and ~ 20900 cm^{-1}) have been assigned to spin-forbidden $d-d$ transitions in
86 octahedrally and/or tetrahedrally coordinated Fe^{3+} , i.e. $^{\text{VI}}\text{Fe}^{3+}$ and $^{\text{IV}}\text{Fe}^{3+}$ respectively (Taran et al.
87 2005).

88 From the optical absorption spectra of ternary solid solution spinels (spinel s.s.-hercynite-
89 gahnite) it is obvious that the color of the mineral depends on the relative intensity of the UV-
90 absorption edge and the absorption bands occurring at energies below 18000 cm^{-1} . Blue and violet
91 colored samples show spectra with weak UV-absorption and consequently they are highly transparent
92 for blue and violet light. The spectra of green colored spinels display strong UV-absorption edges in
93 combination with intensified absorption below 18000 cm^{-1} , thereby defining a transmission window in
94 the green part of the visible spectrum. These two color varieties correspond to the two spinel groups
95 defined by Taran et al. (2005) on the basis of their optical absorption spectra.

96 Assignments of the absorption bands recorded in the low energy range of the visible spectrum
97 and in the high-energy range of the NIR spectrum, between 6000 and 18000 cm^{-1} , are more
98 controversial. Most authors agree that several of these bands are caused by electronic transitions in
99 exchange coupled pairs (ECP) of Fe^{2+} and Fe^{3+} cations or by Fe^{2+} - Fe^{3+} intervalence charge transfer
100 (IVCT) transitions. However, there exists no consensus regarding the precise cation pair configurations
101 responsible for the various absorption bands recorded in this region. Taran et al. (2005) ascribed this to
102 different Fe^{3+} and Fe^{2+} ordering in the spinel samples studied by different authors. Their remark
103 underlines the importance of detailed characterization, including site occupancy data, of samples used
104 in spectroscopic studies. In this context it is interesting to note that information on cation site
105 occupancies are with only two exceptions (Hålenius et al. 2002; D'Ippolito et al. 2013) missing in
106 published spectroscopic studies on the spinel-gahnite-hercynite ternary. As the study by Hålenius et al.

107 (2002) was exclusively based on synthetic samples and the study by D'Ippolito et al. (2013) concerned
108 merely a single natural sample, the need for spectroscopic data on additional natural samples that have
109 been carefully characterized is obvious. In particular, as pointed out by Taran et al. (2005), the fact that
110 electronic transitions in different iron cations ($^{IV}\text{Fe}^{2+}$, $^{VI}\text{Fe}^{2+}$, $^{IV}\text{Fe}^{3+}$ and $^{VI}\text{Fe}^{3+}$) may result in absorption
111 bands at comparable energies makes band assignments in the absence of structural and site occupancy
112 information difficult. Hence, in the present study we have collected optical absorption spectra on four
113 natural samples of Fe-bearing spinels that we have characterized in detail by using electron
114 microprobe, Mössbauer spectroscopy and single crystal X-ray diffraction techniques. The aim of this
115 study was to improve the interpretation of optical absorption spectra of iron-bearing spinels and in
116 particular evaluate the various existing assignments of the optical absorption bands between ~ 6000 and
117 $\sim 18000 \text{ cm}^{-1}$.

118

119 **Samples and experimental methods**

120 Four natural gahnite crystals have been analyzed by electron microprobe analysis (EMPA), Mössbauer
121 spectroscopy (MS), single crystal X-ray diffraction structural refinement (SREF), optical absorption
122 spectroscopy (OAS), and Fourier transform infrared spectroscopy (FTIR). The specimens belong to the
123 mineral collection of the Earth Sciences Museum, University of Bari, and are labeled Ni8967d,
124 Ni8967e, Sp2781_6a, Sp2781_6c. They were loose single crystals with octahedral habitus and original
125 dimensions $2.8 \times 2.8 \times 1.3 \text{ mm}$, $4.2 \times 3.8 \times 3.5 \text{ mm}$, $2.3 \times 2.3 \times 1.9 \text{ mm}$, and $1.6 \times 1.4 \times 1.1 \text{ mm}$,
126 respectively. The crystals are transparent and blue to green colored: Ni8967d is pale blue, Ni8967e and
127 Sp2781_6a are blue, and Sp2781_6c is dark green. The specimens are from two different localities:
128 Ni8967d and Ni8967e originate from pegmatite pockets of Jemaa, Kaduna state, Nigeria, whereas
129 Sp2781_6a and Sp2781_6c come from the Cu(-Ni-Fe) ore of the Migliandone mine, Val d'Ossola, Italy.

130

131 *Electron microprobe analysis*

132 Spinel crystals were mounted in epoxy discs, thinned, polished, and carbon coated for electron
133 microprobe analysis (EMPA, WDS method) on a Cameca SX 50 instrument at CNR-IGAG laboratory
134 c/o Sapienza University of Rome, operating at an accelerating potential of 15 kV and a sample current
135 of 15 nA, with an incident beam size of $\approx 1 \mu\text{m}$. Synthetic and natural standards used were corundum
136 (Al), magnetite (Fe), wollastonite (Si), rutile (Ti), vanadinite (V), metallic Zn, Mn, Co and Ni. A PAP
137 CAMECA program (Pouchou and Pichoir 1984) was used for raw data reduction. Up to eight spot
138 analyses were collected to obtain average chemical compositions.

139

140 *Mössbauer spectroscopy*

141 The gahnite samples were studied by Mössbauer spectroscopy in order to gain information on the
142 oxidation state and site distribution of Fe. Spectra were acquired at room temperature using a
143 conventional spectrometer system operated in constant acceleration mode, with a nominally 50 mCi
144 ^{57}Co source in Rh matrix and a 1024 channel data storage module. Absorbers were prepared by mixing
145 10-24 g grinded sample material with an acrylic resin and pressing to 12-mm discs under moderate
146 heating. Spectra measured in the range -4.5 to +4.5 mm/s were calibrated and folded against an $\alpha\text{-Fe}$
147 foil, and then further reduced to 256 channels before fitting using the least-squares fitting software
148 MDA (Jernberg and Sundqvist 1983) assuming Lorentzian absorption lines. A relatively simple fitting
149 model consisting of one doublet for Fe^{2+} and one doublet for Fe^{3+} was applied to fit the spectra of the
150 Fe-poor samples (Ni8967d, Ni8967e, Sp2781_6a), whereas a third doublet was added to fit the
151 spectrum of the most Fe-rich sample (Sp2781_6c).

152

153 *Single crystal X-ray diffraction structural refinement*

154 X-ray diffraction measurements were performed at the Earth Sciences Department, Sapienza University
155 of Rome, with a Bruker KAPPA APEX-II single-crystal diffractometer, equipped with a CCD area
156 detector ($6.2 \times 6.2 \text{ cm}^2$ active detection area, 512×512 pixels) and a graphite crystal
157 monochromator, using $\text{MoK}\alpha$ radiation from a fine-focus sealed X-ray tube. The sample-to-detector
158 distance was 4 cm. A total of 1613-1695 exposures per sample (step = 0.2° , time/step = 10 s) covering
159 the full reciprocal sphere were collected. Final unit-cell parameters were refined by using the Bruker
160 AXS SAINT program from about 800 recorded reflections with $I > 10 \sigma_I$ in the range $8^\circ < 2\theta < 91^\circ$.
161 The intensity data were processed and corrected for Lorentz, polarization and background effects with
162 the APEX2 software program of Bruker AXS. The data were corrected for absorption using multi-scan
163 method (SADABS). The absorption correction led to a significant improvement in R_{int} . No violation of
164 $Fd\bar{3}m$ symmetry was noted. Sporadic appearance of forbidden space-group reflections was recognized
165 as double reflections.

166 Structural refinements were done with the SHELXL program (Sheldrick 2008). Setting the origin at
167 $\bar{3}m$, initial atomic positions for oxygen atoms were taken from Bosi et al. (2010) and Fregola et al.
168 (2011). Variable parameters were overall scale factor, extinction coefficient, atomic coordinates, site
169 scattering values expressed as mean atomic number (m.a.n.), and atomic displacement factors. No
170 chemical constraint was applied during the refinement. To obtain the best values of statistical indexes
171 ($R1$ and $wR2$) the M site was modeled considering the presence of Al, whereas the T site was modeled
172 by Zn in all samples, except for sample Sp2781_6c modeled by Zn vs. Fe. Three full-matrix refinement
173 cycles with isotropic displacement parameters for all atoms were followed by anisotropic cycles until
174 convergence was attained (that is, when the shifts for all refined parameters were less than their
175 estimated standard deviation).

176

177 *Optical absorption spectroscopy and Fourier transform infrared spectroscopy*

178 Unpolarized, room-temperature optical absorption spectra in the spectral range 270-1100 nm (37037-
179 9091 cm^{-1}) were recorded on doubly sided polished single crystal sections at a spectral resolution of 1
180 nm using a AVASPEC-ULS2048X16 spectrometer attached via a 400 μm UV fiber cable to a Zeiss
181 Axiotron UV-microscope. A 75 W Xenon arc was used as a light source and Zeiss Ultrafluar 10 \times
182 lenses served as objective and condenser. The size of the circular measure aperture was 64 μm in
183 diameter. The wavelength scale of the spectrometer was calibrated against Ho_2O_3 doped and
184 $\text{Pr}_2\text{O}_3/\text{Nd}_2\text{O}_3$ doped standards (Hellma glass filters 666F1 and 666F7) with accuracy better than 15 cm^{-1}
185 in the wavelength range 300-1100 nm.

186 Absorption spectra were measured in the near-infrared range using a Bruker Equinox 55 FTIR
187 spectrometer equipped with a halogen lamp source, a CaF_2 beam-splitter and an InSb detector. Sample
188 absorbers consisted of doubly sided polished crystal sections with thicknesses of 24-68 μm , which were
189 placed over stain-less steel apertures with diameters of 100-400 μm . A total of at least 200 scans were
190 acquired for each sample over the spectral range 2000-13000 cm^{-1} with a resolution of 4 cm^{-1} .
191 Recorded spectra were fitted using the Jandel PeakFit 4.12 software assuming Gaussian peak shapes.

192

193 **Results and Discussion**

194 *Crystal chemistry of the samples*

195 Electron microprobe analyses revealed that the chemical composition of the present gahnite crystals is
196 almost homogeneous within each crystal. Neither chemical nor color zoning was observed.
197 Nevertheless, two distinct sets of data were acquired, the first from the original, entire samples, the
198 second from those portions of crystals that were used for spectroscopic and structural analyses. The two
199 datasets are in good agreement and results of the second set are summarized in Table 1. It shows that
200 all the analyzed crystals contain Al, Zn and Fe as major components, and thus belong to the join
201 gahnite-hercynite.

202

203 *Fe³⁺/Fe_{tot} ratios and Fe site distribution*

204 The recorded Mössbauer spectra (Fig. 1) are all dominated by an un-split or slightly split absorption
205 band centered at 0.91 mm/s, which could be adequately fitted with one absorption doublet with
206 quadrupole splitting values ranging from 0.13 to 0.32 mm/s (Table 2). These parameters are typical for
207 Fe²⁺ in the highly symmetric T position (^{IV}Fe²⁺) in an ordered spinel structure (Waerenborgh et al.
208 1990, 1994a; Lenaz et al. 2004), with slightly increasing quadrupole splitting values coupled to next-
209 nearest neighbour effects (e.g. Waerenborgh et al. 1990) with increasing Fe content. The dominance of
210 this doublet show that Fe mainly occurs as ^{IV}Fe²⁺ in the studied samples, although minor amounts (a
211 few percent of the total Fe-content) of octahedrally coordinated Fe²⁺ (^{VI}Fe²⁺) cannot be excluded. For
212 the most Fe-rich sample Sp2781_6c this main band show a slight broadening, and since OAS and
213 structure refinement data (below) indicate low amounts of ^{VI}Fe²⁺, an additional doublet with higher
214 quadrupole splitting was fitted to this spectrum. The obtained hyperfine parameters (Table 2) are
215 similar to those obtained for ^{VI}Fe²⁺ by Waerenborgh et al. (1994a) on synthetic Fe-containing gahnite,
216 and indicate an ^{VI}Fe²⁺/Fe_{tot} ratio of approximately 4 %.

217 In addition to the Fe²⁺ doublets, all spectra display a minor shoulder on the low-velocity side of
218 the main band. Two fitting models were tested to fit the weak absorption: one with a relatively low
219 centroid shift (0.21-0.27 mm/s) typical for tetrahedrally coordinated Fe³⁺ (^{IV}Fe³⁺), and one with a larger
220 centroid shift (0.32-0.38 mm/s) indicative of octahedrally coordinated Fe³⁺ (^{VI}Fe³⁺). In line with
221 previous Mössbauer studies on natural and synthetic gahnite (Waerenborgh et al. 1990, 1994b) we
222 consider the model with the higher centroid shift, and hence Fe³⁺ predominantly in the M site, to be the
223 more appropriate (Fig. 1). However, both models resulted in appropriate fits and show only minor
224 deviations in individual Fe³⁺/Fe_{tot} ratios, which are within the expected error limits, with the exception
225 of sample Ni8967d that showed a 5% lower Fe³⁺/Fe_{tot} ratio for the fitting model with the lower centroid

10

226 shift. The obtained $\text{Fe}^{3+}/\text{Fe}_{\text{tot}}$ ratios increase from 2.8 % for the most Fe-rich sample to 29.6 % for the
227 sample with the lowest Fe-concentration (Table 2), which means that the Fe^{3+} content per formula unit
228 is relatively constant for the four samples as it ranges between 0.005-0.011 apfu (Table 1).

229

230 *Structural characterization and cation distribution*

231 Results of X-ray diffraction structural refinements of the four studied crystals are listed in Table 3, and
232 intracrystalline cation distributions are reported in Table 4. The cation distributions were obtained by
233 an optimization program applying a minimization function in which both structural and chemical data
234 (such as bond lengths and site-scattering in terms of equivalent electrons, i.e., m.a.n.) are taken into
235 account. The minimization procedure has been presented and discussed previously (Carbonin et al.
236 1996; Andreozzi et al. 2001; Lavina et al. 2002; Bosi et al. 2004; Lenaz and Princivalle 2011; Della
237 Giusta et al. 2011). T-O and M-O bond distances were calculated as the linear contribution of each
238 cation multiplied by its specific bond length, the latter refined on the basis of analysis of more than 250
239 spinel structural data from the literature (Lavina et al. 2002), except for $^{\text{IV}}\text{Zn-O} = 1.949(1) \text{ \AA}$ which
240 was refined by Bosi et al. (2011). In the present case Zn^{2+} and Fe^{3+} were constrained at the T and M
241 site, respectively, the former in agreement with Zn site preference, the latter in agreement with
242 Mössbauer and OAS evidences, and very small amounts of Mg may occur at the M site.

243 In the examined spinel samples the a parameter increases from 8.0912(2) \AA to 8.1103(2) \AA with
244 increasing iron content, and the tetrahedral bond distance T-O increases from 1.9499(6) to 1.9582(6) \AA ,
245 whereas M-O keeps almost constant, increasing from 1.9153(3) to 1.9179(3) \AA . Keeping in mind the
246 effective ionic radii for $^{\text{IV}}\text{Zn}^{2+}$, $^{\text{IV}}\text{Fe}^{2+}$, $^{\text{VI}}\text{Al}^{3+}$, and $^{\text{VI}}\text{Fe}^{2+}$ (0.60, 0.63, 0.535, 0.61 \AA , respectively,
247 Shannon 1976), this would indicate that Fe^{2+} preferentially substitutes for Zn at the T site, but also that
248 some Fe^{2+} substitutes for Al at the M site in the dark green sample. This is confirmed by the structural
249 formulae obtained by combining SREF, Mössbauer and EMPA data (Table 4). The inversion parameter

250 *i* increases with the total iron content, from zero for the pale blue sample Ni8967d to ca. 0.06 for the
251 dark green sample Sp2781_6c. This result is in agreement with what was previously found for the
252 synthetic $Zn_{1-x}Fe_xAl_2O_4$ solid solution series by Waerenborgh et al. (1994a).

253

254 *Optical absorption spectroscopy and Fourier transform infrared spectroscopy*

255 The optical absorption spectra of our four natural blue to green colored gahnite samples acquired in the
256 range 33000-9000 cm^{-1} are shown in Figures 2a and 2b, whereas fitted absorption bands and their
257 energies, widths and intensities are illustrated in Figure 3 and reported in Table 5. All spectra are
258 composed of at least 12 peaks labeled from *a* to *l*. As already observed by Taran et al. (2005), the most
259 significant differences between spectra of green and blue spinel samples are a more intense UV-edge
260 that extends further into the visible spectral region and overall stronger absorption bands, in particular
261 at energies below $\sim 18000\text{ cm}^{-1}$, for the green spinel. This correlates with the higher total iron contents
262 recorded in our green sample (0.295 apfu), as compared to the blue ones (0.041-0.100 apfu). However,
263 some band intensity ratios in spectra of the blue samples are very different from those recorded in the
264 spectrum of the green sample. In particular, the low-energy absorption bands *j*, *k* and *l* are distinctly
265 enhanced in spectra of our green sample. This demonstrates that differences in the optical absorption
266 spectra of the blue and green samples are not entirely explained by differences in total Fe-contents, but
267 also iron valency and site distributions are important.

268 In detail, we interpret the fitted absorption bands above $\sim 18000\text{ cm}^{-1}$ in spectra of samples
269 Ni8967d, Ni8967e and Sp2781_6a in accordance with assignments presented in previous optical
270 absorption spectroscopic studies of Fe^{2+} -dominant crystals within the spinel-hercynite-gahnite ternary
271 (Slack 1964; Gaffney 1973; Dickson and Smith 1976; Schmetzer et al. 1989; Taran et al. 2005).
272 Consequently, we assign absorption bands *a*, *b*, *c*, *d*, *e* and *f* in these samples to spin-forbidden
273 electronic *d-d* transitions in tetrahedrally coordinated Fe^{2+} . This is consistent with a linear dependence

274 of their intensities on the sample $^{IV}\text{Fe}^{2+}$ -concentration as determined by electron microprobe,
275 Mössbauer spectroscopy and X-ray single crystal refinement techniques. In the spectrum of the Fe-rich
276 sample Sp2781_6c we observe enhancements of the intensities of the bands *c* to *f*, especially of *d* and *e*
277 (Table 5), suggesting that they are partly due to $^{IV}\text{Fe}^{2+}$ -related exchange coupled pair (ECP) transitions
278 in this sample. It has previously been suggested that bands occurring at similar positions to those of our
279 bands *e* and *f* can be caused by spin-forbidden *d-d* transitions in octahedrally ($^{VI}\text{Fe}^{3+}$) and/or
280 tetrahedrally ($^{IV}\text{Fe}^{3+}$) coordinated ferric iron (Taran et al. 2005) or by electronic transitions in exchange
281 coupled pairs of $^{IV}\text{Fe}^{3+}$ and $^{VI}\text{Fe}^{3+}$ (Andreozzi et al. 2001). Anyway, the low Fe^{3+} concentrations in our
282 samples rule out intensified absorption in this region due to overlapping bands caused by spin-
283 forbidden single ion transitions. The exact determination of which $^{IV}\text{Fe}^{2+}$ -related ECP transition, i.e.
284 $^{IV}\text{Fe}^{2+}$ - $^{IV}\text{Fe}^{3+}$, $^{IV}\text{Fe}^{2+}$ - $^{VI}\text{Fe}^{3+}$, $^{IV}\text{Fe}^{2+}$ - $^{IV}\text{Fe}^{2+}$ or $^{IV}\text{Fe}^{2+}$ - $^{VI}\text{Fe}^{2+}$ pair transition, is responsible for the
285 intensifications of bands *c* to *f* that we observe, cannot be done from the present study. Further studies
286 on a considerably larger set of samples with well-characterized cation occupancies are needed.

287 The absorption bands *g*, *h* and *i* are observed at ~ 18200 , ~ 17100 and ~ 15950 - 16000 cm^{-1} in
288 optical spectra of all our four samples. However, these bands are more distinct and better resolved in
289 the spectra of the three low-Fe crystals than in the green sample Sp2781_6c with a ca. three times
290 higher Fe-content. The bands are characterized by moderate bandwidths ($\omega_{1/2} \sim 1000$ - 1600 cm^{-1}) and
291 their intensities do not show linear Beer's law relations to the sample $^{IV}\text{Fe}^{2+}$ -contents. Previously
292 published optical absorption spectra of spinel-hercynite-gahnite solid solution crystals have also
293 recorded absorption bands in this region. Slack (1964) observed only one band at 18100 cm^{-1} , which he
294 assigned to a spin-allowed transition in $^{VI}\text{Cr}^{3+}$. Gaffney (1973) later reassigned this band to the spin-
295 forbidden transition $^5\text{E}(\text{D}) \rightarrow ^3\text{T}_1(\text{H})$ in $^{IV}\text{Fe}^{2+}$. Dickson and Smith (1976) recorded at room temperature
296 three bands in this spectral region at ~ 15800 , ~ 17300 and ~ 18050 cm^{-1} . They assigned the latter band,
297 in accordance with Gaffney (1973), to a spin-forbidden transition in $^{IV}\text{Fe}^{2+}$, but noted that they could

298 not offer any definite assignment for the remaining two bands. Taran et al. (2005) fitted five absorption
299 bands in the 17200-20500 cm^{-1} region to their spinel spectra. Among these, two bands were located at
300 ~ 17200 and 18000 cm^{-1} . They did not observe any absorption band at $\sim 15950 \text{ cm}^{-1}$. Taran et al. (2005)
301 concluded that the origin of the band system in the 17200-20500 cm^{-1} region “is not quite clear”, but “it
302 is very likely that some of them are caused by spin-forbidden transitions of $^{\text{IV}}\text{Fe}^{2+}$ ”. They also assumed
303 that “some of them may be due to the presence of trace amounts of tetrahedral Co^{2+} ”. In view of the
304 fact that our spectra revealed a well-resolved absorption band at ~ 15950 - 16000 cm^{-1} which has not
305 been previously recorded in spectra of Fe-bearing gahnite, and that an absorption band at a similar
306 position ($\sim 16000 \text{ cm}^{-1}$) was observed in natural Co- and Fe-bearing spinels and assigned to a spin-
307 allowed transition of $^{\text{IV}}\text{Co}^{2+}$ (Schmetzer et al. 1989), we decided to explore whether trace amount of
308 $^{\text{IV}}\text{Co}^{2+}$ at levels below the detection limits of the electron microprobe analyses may be the cause for the
309 band system. The optical absorption spectra of synthetic single crystals on the MgAl_2O_4 - CoAl_2O_4 join
310 show a set of absorption bands caused by the split spin-allowed $^4\text{A}_2(\text{F}) \rightarrow ^4\text{T}_1(\text{P})$ transition in $^{\text{IV}}\text{Co}^{2+}$
311 and superimposed spin-forbidden $^{\text{IV}}\text{Co}^{2+}$ -bands in this spectral region (Bosi et al. 2012). The molar
312 absorption coefficient (ϵ) of this band is extremely high, $\sim 200 \text{ l/mol}\cdot\text{cm}$. Actually the band energies,
313 band widths and band intensity ratios of the three bands *g*, *h* and *i* that we observe in the present spectra
314 of blue gahnites are identical to what we record in spectra of Co-doped spinel s.s.. The absorption
315 envelope in the 15950 - 18200 cm^{-1} spectral region is reproduced with high precision by a spectrum of a
316 MgAl_2O_4 spinel containing ca. 200 ppm of Co^{2+} , as calculated from the band parameters in Bosi et al.
317 (2012), with a minor, but significant, deviation in the high energy end of the band system (i.e., at
318 $\sim 18200 \text{ cm}^{-1}$) that displays a marginally higher relative intensity in our natural samples. This is most
319 likely caused by the presence of a partly overlapping, but weaker band caused by the $^5\text{E}(\text{D}) \rightarrow ^3\text{T}_1(\text{H})$
320 transition in $^{\text{IV}}\text{Fe}^{2+}$ (e.g., Gaffney 1973).

321 The bands *j* and *k* are present in the optical spectra of all our four samples, but they exhibit
322 increased relative intensities in the spectrum of the green sample. The band *j* at $\sim 14700\text{ cm}^{-1}$ is
323 dominant in the optical spectrum of the dark green sample Sp2781_6c and its intensity correlates in a
324 highly non-linear manner with the sample $^{\text{IV}}\text{Fe}^{2+}$ -concentration (Fig. 4). This indicates that this
325 absorption band is related to an electronic transition in a cation pair. SREF and MS data suggest that
326 the contents of $^{\text{IV}}\text{Fe}^{3+}$ as well as $^{\text{VI}}\text{Fe}^{2+}$ are negligible or very low in our samples. This, in addition to the
327 fact that Fe^{2+} - Fe^{3+} IVCT processes in oxygen-based minerals preferably occur in clusters of cations
328 located in edge- or face-sharing sites (Mattson and Rossman 1987), reduce the likelihood for Fe^{2+} - Fe^{3+}
329 IVCT in the present samples. The transition $^{\text{VI}}\text{Fe}^{2+}$ - $^{\text{VI}}\text{Fe}^{3+}$ IVCT, even if possible, would be highly
330 unlikely in our case due to the very low $^{\text{VI}}\text{Fe}^{2+}$ -content of the green sample (0.04 apfu) as compared to
331 its $^{\text{IV}}\text{Fe}^{2+}$ -content (0.25 apfu). On the other hand, exchange-coupled pairs, in which the participating
332 ions are located at sites that share faces, edges, or just corners, can act in the spinel structure (Hålenius
333 et al. 2002; Hålenius and Bosi 2014). These observations strongly suggest an electronic transition in
334 exchange coupled $^{\text{VI}}\text{Fe}^{3+}$ - $^{\text{IV}}\text{Fe}^{2+}$ cation pairs as the origin of the *j* band. Hence, our data support the
335 interpretation by Taran et al. (2005) that was exclusively based on spectroscopic data obtained at
336 variable temperatures and pressure without supporting cation occupancy data. Moreover, this band *j* is
337 broad, as its full width at half maximum is $\omega_{1/2} \sim 2500\text{ cm}^{-1}$, and this is a further argument in favor of
338 the suggestion by Taran et al. (2005) that it represents the spin-forbidden $^6\text{A}_{1g} \rightarrow ^4\text{T}_{2g}$ transition of
339 $^{\text{VI}}\text{Fe}^{3+}$, intensified by exchange coupling interaction in $^{\text{VI}}\text{Fe}^{3+}$ - $^{\text{IV}}\text{Fe}^{2+}$ pairs.

340 The origin of the absorption band *k* at $\sim 12500\text{ cm}^{-1}$ is problematic. Taran et al. (2005) suggested
341 that this band had a similar origin as the *j* band, i.e., it is caused by a spin-forbidden $^6\text{A}_{1g} \rightarrow ^4\text{T}_{1g}$
342 transition in $^{\text{VI}}\text{Fe}^{3+}$ that is intensified by exchange coupling interaction in $^{\text{VI}}\text{Fe}^{3+}$ - $^{\text{IV}}\text{Fe}^{2+}$ pairs. From our
343 spectra we observe that the intensity of this band deviates from a Beer's law relationship with $^{\text{IV}}\text{Fe}^{2+}$

344 (Fig. 4) and, consequently, we agree that the band may be caused by the process suggested by Taran et
345 al. (2005).

346 The absorption band *l* at $\sim 10500\text{ cm}^{-1}$ is a prominent feature in the spectrum of the green sample
347 Sp2781_6c, which is the only sample that contains concentrations of VI Fe^{2+} in amounts detectable by
348 single crystal structure analysis. In the spectra of the three remaining crystals this band is barely
349 discernable. This band has previously been assigned to a spin-allowed ${}^5\text{T}_{2g} \rightarrow {}^5\text{E}_g$ transition of VI Fe^{2+}
350 (e.g., Gaffney 1973; Dickson and Smith 1976; Schmetzer et al. 1989) or alternatively to the spin-
351 forbidden ${}^6\text{A}_{1g} \rightarrow {}^4\text{T}_{1g}$ transition of VI Fe^{3+} intensified by the VI Fe^{3+} - IV Fe^{2+} exchange interaction (Taran
352 et al. 2005). The fact that this band becomes a prominent feature only in the spectrum of our sample
353 that contains appreciable VI Fe^{2+} -contents speaks in favor of the former assignment.

354 Finally, the complex band centered at about 5000 cm^{-1} (Fig. 5) is related to the spin allowed *d-d*
355 electronic transition ${}^5\text{E} \rightarrow {}^5\text{T}_2$ in IV Fe^{2+} that is split into four components (*m*, *n*, *o*, *p*) due to dynamic
356 Jahn-Teller effect (e.g., Skogby and Hålenius 2003). Moving from the pale blue, through the blue (both
357 blue crystals with similar band-height), to the dark green crystal, the intensity of the band increases,
358 reflecting increasing IV Fe^{2+} -contents. The very limited shifts in the position of the *n* (from 4760 to 4800
359 cm^{-1}) and *p* bands (from 3640 to 3690 cm^{-1}) confirm the strong relaxation of T-O bonds observed
360 previously in various spinel solid solution series (Skogby and Hålenius 2003; Hålenius et al. 2010;
361 Hålenius et al. 2011; Bosi et al. 2012).

362

363

Implications

364 In the present study, the causes for color variations in four natural Fe-bearing gahnite samples have
365 been determined using optical absorption spectroscopy data supported by information on iron valency
366 and site distribution. The latter information have been demonstrated to be crucial for interpreting
367 optical absorption spectra. Electronic transitions in a trace element chromophore (IV Co^{2+}) at levels

368 below the detection limit of the electron microprobe are shown to contribute to light absorption. These
369 findings are of interest not only to the community of researchers studying spinel oxide minerals from a
370 geological point of view, but also to those involved in the general topic of coloration of minerals and
371 crystalline materials.

372 In gemology, for example, the physics and chemistry of gemstone coloration is an important
373 subject of study (e.g., Nassau 2001) as well as a central element concurring to their pricing. The
374 presence of certain chromophores (especially in trace concentrations) may be exploited to reveal
375 gemstones provenance, which can be of interest for commercial (or even forensic) purposes.

376 In the field of production of industrial materials with certain color characteristics, as for the case
377 of gahnite in glazed tiles or for ceramic pigments in general, the results obtained in the present work
378 may help to a better understanding of the role of ceramic colorants in a glaze. Spinel-based materials
379 are used to obtain blue and green ceramic pigments, as the blue pigment consisting of corundum and
380 Ti-bearing hercynite, or the cobalt-zinc-alumina-chromite system where a range of colors from green to
381 blue-green and blue can be obtained by varying the amounts of cobalt and chrome oxides (Andreozzi et
382 al. 2004; Di Benedetto et al. 2006).

383

384

385

Acknowledgments

386 Alessandro Monno is thanked for having kindly made available the analyzed samples. Marcello
387 Serracino kindly assisted during electron microprobe analysis. This paper partly benefited from the
388 SYNTHESYS SE-TAF-893 grant of the European Community, Research Infrastructure Action, FP7
389 CAPACITIES Programme, to RAF. We greatly appreciate the useful comments by two anonymous
390 reviewers as well as the efficient handling of the manuscript by the associate editor Kristina Lilova.

391

392

References cited

- 393 Anderson, B.W., and Payne, C.J. (1937) Magnesium-zinc-spinels from Ceylon. Mineralogical
394 Magazine, 24, 547-554.
- 395 Andreozzi, G.B., Hålenius, U., and Skogby, H. (2001) Spectroscopic active $^{IV}Fe^{3+}$ - $^{VI}Fe^{3+}$ clusters in
396 spinel-magnesioferrite solid solution crystals: a potential monitor for ordering in oxide spinels.
397 Physics and Chemistry of Minerals, 28, 435-444.
- 398 Andreozzi, G.B., Baldi, G., Bernardini, G.P., Di Benedetto, F., and Romanelli, M. (2004) ^{57}Fe
399 Mössbauer and electronic spectroscopy study on a new synthetic hercynite-based pigment.
400 Journal of the European Ceramic Society, 24, 821-824.
- 401 Appel, P.W.U. (2000) Gahnite in the ~3.75 Ga Isua Greenstone Belt, West Greenland. Mineralogical
402 Magazine, 64, 121-124.
- 403 Bosi, F., Andreozzi, G.B., Ferrini, V., and Lucchesi, S. (2004) Behavior of cation vacancy in
404 kenotetrahedral Cr-spinels from Albanian eastern belt ophiolites. American Mineralogist, 89,
405 1367–1373.
- 406 Bosi, F., Hålenius, U., and Skogby, H. (2010) Crystal chemistry of the $MgAl_2O_4$ - $MgMn_2O_4$ - $MnMn_2O_4$
407 system: Analysis of structural distortion in spinel and hausmannite-type structures. American
408 Mineralogist, 95, 602–607.
- 409 Bosi, F., Andreozzi, G.B., Hålenius, U., and Skogby, H. (2011) Zn-O tetrahedral bond length variations
410 in normal spinel oxides. American Mineralogist, 96, 594–598.
- 411 Bosi, F., Hålenius, U., D’Ippolito, V. and Andreozzi, G. B. (2012) Blue spinel crystals in the $MgAl_2O_4$ -
412 $CoAl_2O_4$ series: Part II. Cation ordering over short-range and long-range scales. American
413 Mineralogist, 97, 1834-1840.
- 414 Carbonin, S., Russo, U., and Della Giusta, A. (1996) Cation distribution in some natural spinels from
415 X-ray diffraction and Mossbauer spectroscopy. Mineralogical Magazine, 60, 355–368.

- 416 Della Giusta, A., Carbonin, S., and Russo, U. (2011) Chromite to magnetite transformation:
417 compositional variations and cation distributions (Southern Aosta Valley, Western Alps, Italy).
418 *Periodico di Mineralogia*, 80, 1–17.
- 419 Di Benedetto, F., Andreozzi, G., Baldi, G., Barzanti, A., Bernardini, G.P., Faso, V., Pardi, L.A, and
420 Romanelli, M. (2006) HF²EPR spectroscopy of Fe(III) impurities in a blue hercynite-based
421 pigment. *Journal of the European Ceramic Society*, 26, 2301-2305.
- 422 Dickson, B. L., and Smith, G. (1976) Low-temperature optical absorption and Mössbauer spectra of
423 staurolite and spinel. *Canadian Mineralogist*, 14, 206-215.
- 424 D'Ippolito, V., Andreozzi, G.B., Bosi, F., Hålenius, U., Mantovani, L., Bersani, D., and Fregola, R.A.
425 (2013) Crystallographic and spectroscopic characterization of a natural Zn-rich spinel
426 approaching the endmember gahnite (ZnAl₂O₄) composition. *Mineralogical Magazine*, 77,
427 2941-2953.
- 428 Escardino, A., Amorós, J.L., Gozalbo, A., Orts, M.J., and Moreno, A. (2000) Gahnite devitrification in
429 ceramic frits: Mechanism and process kinetics. *Journal American Ceramic Society*, 83, 2938–
430 2944.
- 431 Fregola, R.A., Bosi, F., and Skogby, H. (2011) A first report on anion vacancies in a defect MgAl₂O₄
432 natural spinel. *Periodico di Mineralogia*, 80, 27-38.
- 433 Gaffney, E. S. (1973) Spectra of tetrahedral Fe²⁺ in MgAl₂O₄. *Physical Review B*, 8, 3484-3486.
- 434 Hålenius, U., Skogby, H., and Andreozzi, G.B. (2002) Influence of cation distribution on the optical
435 spectra of Fe³⁺-bearing spinel *s.s.*-hercynite crystals: evidence for electron transitions in ^{VI}Fe²⁺-
436 ^{VI}Fe³⁺ clusters. *Physics and Chemistry of Minerals*, 29, 319-330.
- 437 Hålenius, U., Andreozzi, G. B. and Skogby, H. (2010) Structural relaxation around Cr³⁺ and the red-
438 green color change in the spinel (*sensu stricto*)-magnesiochromite (MgAl₂O₄-MgCr₂O₄) and

- 439 gahnite-zincochromite ($\text{ZnAl}_2\text{O}_4\text{-ZnCr}_2\text{O}_4$) solid-solution series. American Mineralogist, 95,
440 456-462.
- 441 Hålenius, U., Bosi, F. and Skogby, H. (2011) A first record of strong structural relaxation of TO_4
442 tetrahedra in a spinel solid solution. American Mineralogist, 96, 617-622.
- 443 Hålenius, U. and Bosi, F. (2014) Color of Mn-bearing gahnite: A first example of electronic transitions
444 in heterovalent exchange coupled $\text{IVMn}^{2+}\text{-VIMn}^{3+}$ pairs in minerals. American Mineralogist, 99,
445 261-266.
- 446 Heimann, A., Spry, P.G., and Teale, G.S. (2005) Zincian spinel associated with metamorphosed
447 Proterozoic base-metal sulphide occurrences, Colorado: A re-evaluation of gahnite composition
448 as a guide in exploration. Canadian Mineralogist, 43, 601-622.
- 449 Henry, D.J., and Dutrow, B.L. (2001) Compositional zoning and element partitioning in nickeloan
450 tourmaline from a metamorphosed karstbauxite from Samos, Greece. American Mineralogist,
451 86, 1130-1142.
- 452 Jackson, B. (1982) Gem quality gahnite from Nigeria. Journal of Gemmology, 18, 265-276.
- 453 Jernberg, P., and Sundqvist, T. (1983) A versatile Mössbauer analysis program. Uppsala University,
454 Institute of Physics, UUIP-1090.
- 455 Lavina, B., Salviulo, G., and Della Giusta, A. (2002) Cation distribution and structure modelling of
456 spinel solid solutions. Physics and Chemistry of Minerals, 29, 10–18.
- 457 Lenaz, D., and Princivalle, F. (2011) First occurrence of titanomagnetites from the websterite dykes
458 within Balmuccia peridotite (Ivrea-Verbano zone): crystal chemistry and structural refinement.
459 Periodico di Mineralogia, 80, 19–26.
- 460 Lenaz, D., Skogby, H., Princivalle, F., and Hålenius, U. (2004) Structural changes and valence states in
461 the $\text{MgCr}_2\text{O}_4\text{-FeCr}_2\text{O}_4$ solid solution series. Physics and Chemistry of Minerals, 31, 633–642.

- 462 Mattson, S.M., and Rossman, G.R. (1987) Identifying characteristics of charge transfer transitions in
463 minerals. *Physics and Chemistry of Minerals*, 14, 94-99.
- 464 Nassau, K. (2001) *The Physics and Chemistry of Color: The Fifteen Causes of Color*. Second edition.
465 Wiley Series in Pure and Applied Optics. Wiley-Interscience; 481 pp.
- 466 O'Neill, H.St.C., and Dollase, W.A. (1994) Crystal structures and cation distributions in simple spinels
467 from powder XRD structural refinements: MgCr_2O_4 , ZnCr_2O_4 , Fe_3O_4 and the temperature
468 dependence of the cation distribution in ZnAl_2O_4 . *Physics and Chemistry of Minerals*, 20, 541-
469 555.
- 470 O'Neill, H.St.C., James, M., Dollase, W.A., and Redfern, S.A.T. (2005) Temperature dependence of
471 the cation distribution in CuAl_2O_4 spinel. *European Journal of Mineralogy*, 17, 581-586.
- 472 Pouchou, J.L., and Pichoir, F. (1984) A new model for quantitative X-ray microanalysis. I. Application
473 to the analysis of homogeneous samples. *La Recherche Aérospatiale*, 3, 167-192.
- 474 Schmetzer, K., Haxel, C., and Amthauer, G. (1989) Colour of natural spinels, gahnospinel and
475 gahnites. *Neues Jahrbuch für Mineralogie Abhandlungen*, 160(2), 159-180.
- 476 Shannon, R.D. (1976) Revised effective ionic radii and systematic studies of interatomic distances in
477 halides and chalcogenides. *Acta Crystallographica*, A32, 751-767.
- 478 Sheldrick, G.M. (2008) A short history of SHELX. *Acta Crystallographica*, A64, 112-122.
- 479 Skogby, H., and Hålenius, U. (2003) An FTIR study of tetrahedrally coordinated ferrous iron in the
480 spinel-hercynite solid solution. *American Mineralogist*, 88, 489-492.
- 481 Slack, G.A. (1964) FeAl_2O_4 - MgAl_2O_4 : Growth and some thermal, optical, and magnetic properties of
482 mixed single crystals. *Physical Review*, 134, A1268-A1280.
- 483 Spry, P.G., and Scott, D.S. (1986) Zincian spinel and staurolite as guides to ore in the Appalachians
484 and Scandinavian Caledonides. *Canadian Mineralogist*, 24, 147-163.

- 485 Taran, M.N., Koch-Müller, M., and Langer, K. (2005) Electronic absorption spectroscopy of natural
486 $(\text{Fe}^{2+}, \text{Fe}^{3+})$ -bearing spinels of spinel s.s.-hercynite and gahnite-hercynite solid solutions at
487 different temperatures and high-pressures. *Physics and Chemistry of Minerals*, 32, 175-188.
- 488 Valenzuela, M.A., Jacobs, J.P., Bosch, P., Reijne, S., Zapata, B., and Brongersma, H.H. (1997) The
489 influence of the preparation method on the surface structure of ZnAl_2O_4 . *Applied Catalysis A:*
490 *General*, 148, 315-324.
- 491 Waerenborgh, J.C., Annersten, H., Ericsson, T., Figueiredo, M.O., and Cabral, J.M.P. (1990) A
492 Mössbauer study of natural gahnite spinels showing strongly temperature-dependent quadrupole
493 splitting distributions. *European Journal of Mineralogy*, 2, 267-271.
- 494 Waerenborgh, J.C., Figueiredo, M.O., Cabral, J.M.P., and Pereira, L.C.J. (1994a) Powder XRD
495 structure refinements and ^{57}Fe Mössbauer effect study of synthetic $\text{Zn}_{1-x}\text{Fe}_x\text{Al}_2\text{O}_4$ ($0 < x \leq 1$)
496 spinels annealed at different temperatures. *Physics and Chemistry of Minerals*, 21, 460-468.
- 497 Waerenborgh, J.C., Figueiredo, M.O., Cabral, J.M.P., and Pereira, L.C.J. (1994b) Temperature and
498 composition dependence of the cation distribution in synthetic $\text{ZnFe}_y\text{Al}_{2-y}\text{O}_4$ ($0 \leq y \leq 1$) spinels.
499 *Journal of Solid State Chemistry*, 111, 300-309.
- 500 Yalçın, Ü., Schreyer, W., and Medenbach, O. (1993) Zn-rich högbomite formed from gahnite in the
501 metabauxites of the Menderas Massif, SW Turkey. *Contributions to Mineralogy and Petrology*,
502 113, 314-324.
- 503

Figure captions

504

505

506 **Figure 1. (a)-(d):** Room temperature Mössbauer spectra of the present Fe-bearing gahnite
507 samples showing raw data (open diamonds), fitted sub-spectra of $^{IV}\text{Fe}^{2+}$ (thin solid line), $^{VI}\text{Fe}^{2+}$ (thin
508 dashed line), $^{VI}\text{Fe}^{3+}$ (thin dotted line) and the total fitted spectrum (bold solid black line).

509

510 **Figure 2.** Optical absorption spectra of our Fe-bearing gahnite samples in the UV-VIS-NIR
511 range (a) and a close-up (b) of the spectra of the three blue colored low-Fe samples in the same spectral
512 range. Peak labels *a* to *l* as referred to in the text and in Table 5.

513

514 **Figure 3.** Net absorption spectrum (UV-edge absorption subtracted) of sample Ni8967e in the
515 UV-VIS-NIR range showing the fitting model used for the optical absorption spectra of all our
516 samples. Measured spectrum as small filled diamonds and fitted bands as thin solid lines. The fitted
517 total spectrum is shown as a thick solid line. Peak labels *a* to *l* as referred to in the text and in Table 5.

518

519 **Figure 4.** A plot of integrated absorption coefficients for the 14700 and 12500 cm^{-1} bands *j* and
520 *k* versus $^{IV}\text{Fe}^{2+}$ -concentrations in our samples.

521

522 **Figure 5.** Optical absorption spectra of our samples in the NIR-MIR range. Peaks labeled *m-p*
523 are discussed in the text.

524

525

526

Tables and table titles

527

TABLE 1. Composition of the present natural iron-bearing gahnite crystals

Sample	Ni8967d	Ni8967e	Sp2781_6a	Sp2781_6c
Al ₂ O ₃ (wt.-%)	54.77(30)	55.03(24)	54.84(62)	54.88(11)
MgO	0.05(1)	0.21(2)	0.19(2)	0.66(1)
MnO	0.09(4)	0.14(6)	0.11(4)	0.37(4)
ZnO	42.97(37)	40.52(36)	39.99(39)	31.16(27)
FeO*	1.18(3)	3.45(7)	3.69(8)	11.27(23)
Fe ₂ O ₃ *	0.49(3)	0.28(7)	0.20(8)	0.31(23)
Total	99.55	99.63	99.02	98.65
Cations on the basis of 4 oxygen atoms				
Al (apfu)	1.983(7)	1.983(7)	1.986(10)	1.974(5)
Mg	0.002(1)	0.010(1)	0.009(1)	0.030(1)
Mn	0.002(1)	0.003(2)	0.002(1)	0.008(1)
Zn	0.974(7)	0.915(6)	0.907(9)	0.702(5)
Fe ²⁺	0.030(1)	0.088(2)	0.095(2)	0.288(6)
Fe ³⁺	0.011(1)	0.007(2)	0.005(2)	0.007(6)
Total	3.002	3.006	3.004	3.009
Gahnite (mol-%)	96.8	90.3	89.7	68.8
Hercynite	3.0	8.7	9.4	28.2
Spinel <i>s.s.</i>	0.2	1.0	0.9	3.0

528

529

530

531

532

533

Notes: wt-% = oxide weight percentages; apfu = atoms per formula unit; * measured by Mössbauer spectroscopy. Standard deviations of several spot analyses and standard errors calculated by error-propagation theory are reported between brackets.

534

535

536

537

TABLE 2. Mössbauer parameters obtained at room temperature

Sample	Int (%)	fwhm (mm/s)	cs (mm/s)	dq (mm/s)	Assignment
Ni8967d	70.4	0.36	0.92	0.13	^{IV} Fe ²⁺
	29.6	0.58	0.32	0.40	^{VI} Fe ³⁺
Ni8967e	92.4	0.36	0.91	0.19	^{IV} Fe ²⁺
	7.6	0.53	0.32	0.39	^{VI} Fe ³⁺
Sp2781_6a	94.8	0.38	0.91	0.17	^{IV} Fe ²⁺
	5.2	0.44	0.38	0.68	^{VI} Fe ³⁺
Sp2781_6c	93.1	0.39	0.91	0.32	^{IV} Fe ²⁺
	4.1	0.31	0.87	0.84	^{VI} Fe ²⁺
	2.8	0.28	0.36	0.91	^{VI} Fe ³⁺

538

539

540

541

542

Notes: Int = percentage of total absorption area; fwhm = full width at half maximum;
cs = centroid shift; dq = quadrupole splitting.

543

544

TABLE 3. Selected X-ray diffraction data for analyzed Fe-bearing gahnite samples

Sample	Ni8967d	Ni8967e	Sp2781_6a	Sp2761_6c
Crystal sizes (mm)	0.24×0.15×0.30	0.18×0.20×0.22	0.18×0.21×0.22	0.19×0.20×0.21
<i>a</i> (Å)	8.0912(2)	8.0954(3)	8.0944(3)	8.1103(2)
<i>u</i>	0.26413(5)	0.26413(6)	0.26420(5)	0.26440(5)
T-O (Å)	1.9499(6)	1.9508(8)	1.9516(7)	1.9582(6)
M-O (Å)	1.9153(3)	1.9163(4)	1.9156(4)	1.9179(3)
T-m.a.n.	29.99(9)	29.68(11)	29.67(9)	28.72(47)
M-m.a.n.	13.12(4)	13.17(5)	13.17(5)	13.19(4)
T- U^{11} (Å ²)	0.00502(7)	0.0044(2)	0.00538(7)	0.00611(8)
M- U^{11} (Å ²)	0.0043(1)	0.0035(1)	0.0046(1)	0.0051(1)
M- U^{12} (Å ²)	-0.00034(6)	-0.00035(7)	-0.00033(7)	-0.00033(6)
O- U^{11} (Å ²)	0.0042(1)	0.0035(2)	0.0045(1)	0.0052(2)
O- U^{12} (Å ²)	-0.0003(1)	-0.0002(1)	-0.0002(1)	-0.00025(9)
Reciprocal range <i>hkl</i>	-12 ≤ <i>h</i> ≤ 16 -14 ≤ <i>k</i> ≤ 11 -11 ≤ <i>l</i> ≤ 16	-14 ≤ <i>h</i> ≤ 14 -15 ≤ <i>k</i> ≤ 15 -15 ≤ <i>l</i> ≤ 7	-15 ≤ <i>h</i> ≤ 13 -15 ≤ <i>k</i> ≤ 14 -10 ≤ <i>l</i> ≤ 14	-13 ≤ <i>h</i> ≤ 13 -14 ≤ <i>k</i> ≤ 8 -15 ≤ <i>l</i> ≤ 15
Set of read reflections	1613	1626	1667	1695
Unique reflections	129	132	125	131
EXTI	0.0104(9)	0.057(2)	0.0120(5)	0.040(2)
<i>R</i> int. (%)	1.03	1.03	0.61	1.84
<i>R</i> 1 (%) all reflections	0.84	1.13	0.95	1.21
<i>wR</i> 2 (%)	2.15	3.01	2.26	2.76
Goof	1.145	1.192	1.211	1.337
Diff. Peaks (±e/Å ³)	-0.21; 0.19	-0.54; 0.44	-0.27; 0.26	-0.46; 0.32

545

546

547

548

549

550

551

552

553

554

555

Notes: *a* = unit-cell parameter; *u* = oxygen fractional coordinate; T-O and M-O = tetrahedral and octahedral bond lengths, respectively; T- and M-m.a.n. = T- and M-mean atomic number; U^{11} = atomic displacement parameter; $U^{11} = U^{22} = U^{33}$ and $U^{12} = U^{13} = U^{23}$ (= 0 for T-site due to symmetry reasons); EXTI = extinction parameter; *R* int. = merging residual value; *R*1 = discrepancy index, calculated from *F*-data; *wR*2 = weighted discrepancy index, calculated from *F*²-data; Goof = goodness of fit; Diff. Peaks = maximum and minimum residual electron density. Radiation, Mo-*K*α = 0.71073 Å. Data collection temperature = 293 K. Total number of frames = 4268. Range for data collection 8° < 2θ < 91°. Origin fixed at $\bar{3}m$. Space group *Fd* $\bar{3}m$. *Z* = 8 formula units. Spinel structure has cations at Wyckoff positions 8*a* ≡ T (1/8, 1/8, 1/8) and 16*d* ≡ M (1/2, 1/2, 1/2), and oxygen anions at 32*e* (*u*, *u*, *u*).

556

557

558

TABLE 4. Structural formulae of the studied natural iron-bearing gahnite crystals

Crystal	Formula
Ni8967d	${}^{\text{IV}}(\text{Zn}_{0.97}\text{Fe}^{2+}_{0.03}) {}^{\text{VI}}(\text{Al}_{1.99}\text{Fe}^{3+}_{0.01})\text{O}_4$
Ni8967e	${}^{\text{IV}}(\text{Zn}_{0.91}\text{Fe}^{2+}_{0.09}) {}^{\text{VI}}(\text{Al}_{1.98}\text{Fe}^{3+}_{0.01}\text{Mg}_{0.01})\text{O}_4$
Sp2781_6a	${}^{\text{IV}}(\text{Zn}_{0.91}\text{Fe}^{2+}_{0.09}) {}^{\text{VI}}(\text{Al}_{1.98}\text{Fe}^{3+}_{0.01}\text{Mg}_{0.01})\text{O}_4$
Sp2781_6c	${}^{\text{IV}}(\text{Zn}_{0.70}\text{Fe}^{2+}_{0.25}\text{Al}_{0.05}) {}^{\text{VI}}(\text{Al}_{1.92}\text{Fe}^{3+}_{0.01}\text{Mg}_{0.03}\text{Fe}^{2+}_{0.04})\text{O}_4$

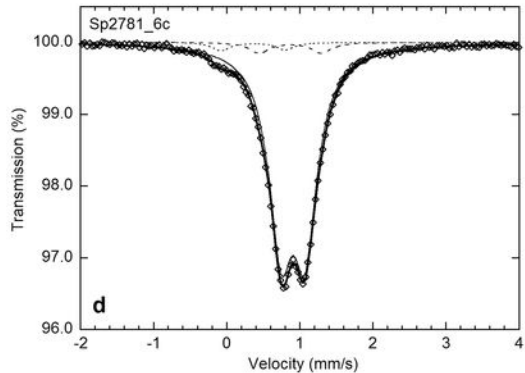
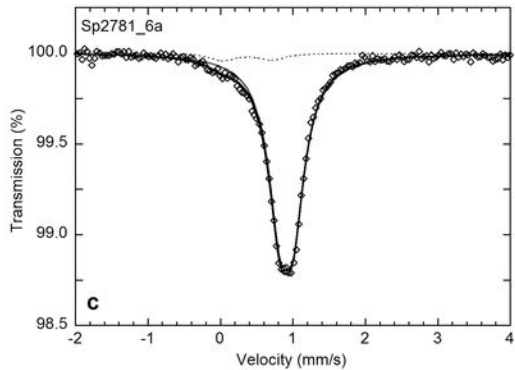
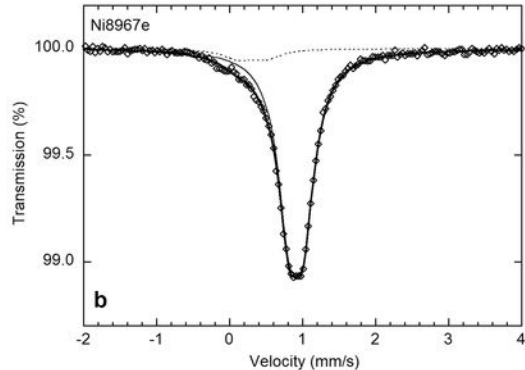
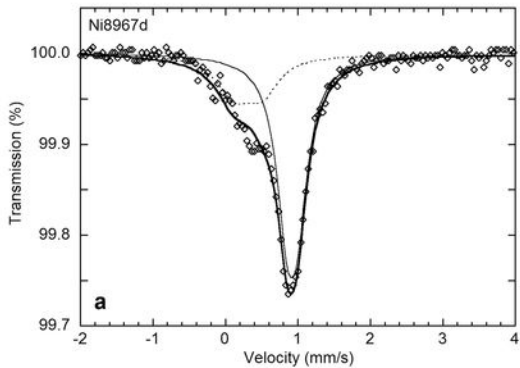
559

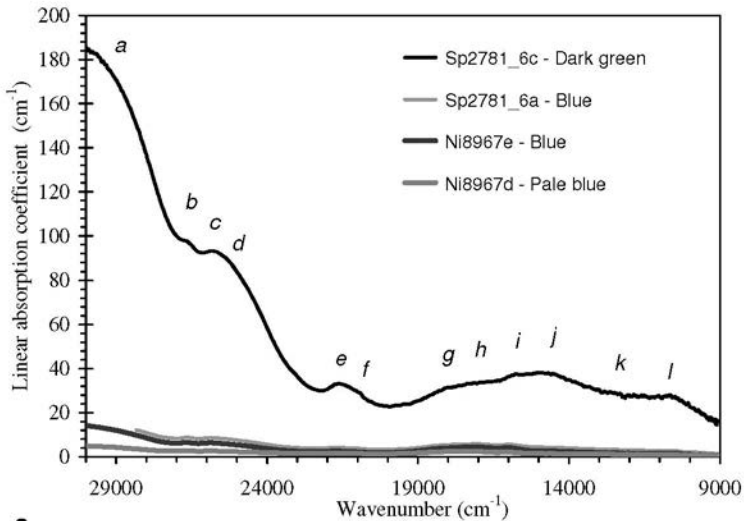
560

561 **TABLE 5.** Parameters and assignments of fitted absorption bands in the UV/VIS/NIR region for the
 562 studied Fe-bearing gahnite samples

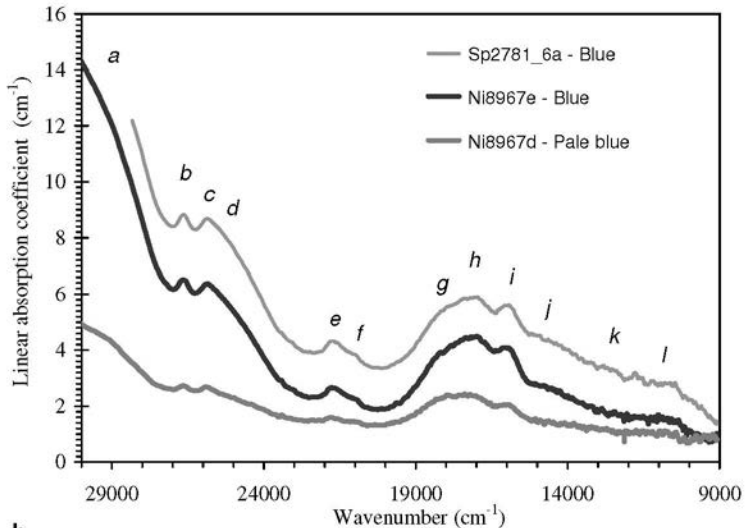
Band	Sample				Assignment	
	Ni8967d	Ni8967e	Sp2781_6a	Sp2781_6c		
	v	29002	28904	nd	nd	
a	$\omega_{1/2}$	940	1085	nd	nd	s.f. $^5E(D) \rightarrow ^3E(D)$ in $^{IV}Fe^{2+}$
	α	0.18	0.72	nd	nd	
	v	26623	26624	26621	26583	
b	$\omega_{1/2}$	415	412	396	319	s.f. $^5E(D) \rightarrow ^3E(D)$ in $^{IV}Fe^{2+}$
	α	0.21	0.57	0.67	2.20	
	v	25868	25871	25856	25840	
c	$\omega_{1/2}$	561	565	577	575	s.f. $^5E(D) \rightarrow ^3T_1(G)$ in $^{IV}Fe^{2+}$ (possibly intensified by ECP, for sample Sp2781_6c)
	α	0.24	0.56	0.56	3.25	
	v	25146	25164	25201	25032	
d	$\omega_{1/2}$	1736	1727	1753	1679	s.f. $^5E(D) \rightarrow ^3T_1(G)$ in $^{IV}Fe^{2+}$ (possibly intensified by ECP, for sample Sp2781_6c)
	α	0.26	1.19	1.49	16.63	
	v	21718	21701	21681	21587	
e	$\omega_{1/2}$	748	730	571	573	s.f. $^5E(D) \rightarrow ^3E(G)$ in $^{IV}Fe^{2+}$ (possibly intensified by ECP, for sample Sp2781_6c)
	α	0.18	0.50	0.58	4.96	
	v	20997	21054	21108	21085	
f	$\omega_{1/2}$	403	529	444	471	s.f. $^5E(D) \rightarrow ^3T_1(P)$ in $^{IV}Fe^{2+}$ (possibly intensified by ECP, for sample Sp2781_6c)
	α	0.10	0.21	0.25	3.02	
	v	18251	18240	18280	18222	
g	$\omega_{1/2}$	1623	1564	1506	1222	s.a. $^4A_2(F) \rightarrow ^4T_1(P)$ in $^{IV}Co^{2+}$ and s.f. $^5E(D) \rightarrow ^3T_1(H)$ in $^{IV}Fe^{2+}$
	α	0.92	1.85	1.85	7.13	
	v	17122	17109	17081	17133	
h	$\omega_{1/2}$	1283	1251	1367	1295	s.a. $^4A_2(F) \rightarrow ^4T_1(P)$ in $^{IV}Co^{2+}$
	α	0.93	2.31	2.42	10.38	
	v	15997	16019	15952	16003	
i	$\omega_{1/2}$	1008	966	988	1019	s.a. $^4A_2(F) \rightarrow ^4T_1(P)$ in $^{IV}Co^{2+}$
	α	0.62	1.71	1.69	6.40	
	v	14763	14749	14820	14788	
j	$\omega_{1/2}$	2501	2531	2587	2300	s.f. $^6A_{1g} \rightarrow ^4T_{2g}$ in $^{VI}Fe^{3+}$ intensified by $^{VI}Fe^{3+}$ - $^{IV}Fe^{2+}$ ECP
	α	0.36	1.19	1.69	16.37	
	v	12687	12480	12560	12513	
k	$\omega_{1/2}$	2230	2291	2303	2330	s.f. $^6A_{1g} \rightarrow ^4T_{1g}$ in $^{VI}Fe^{3+}$ intensified by $^{VI}Fe^{3+}$ - $^{IV}Fe^{2+}$ ECP
	α	0.14	0.38	0.92	8.09	
	v	11018	10801	10663	10773	
l	$\omega_{1/2}$	1034	1036	1177	1259	s.a. $^5T_{2g} \rightarrow ^5E_g$ in $^{VI}Fe^{2+}$
	α	0.17	0.44	0.81	7.77	

563 *Notes:* ν = band position (cm^{-1}); $\omega_{1/2}$ = band width (cm^{-1}); α = linear absorption coefficient (cm^{-1});
564 s.f.= spin-forbidden; s.a.= spin-allowed; nd = not determined
565
566





a



b

